PV Array Reconfiguration Based on the Shaded Cells' Number for PV Modules

Jun Qi, Xun Huang, Beijia Ye, and Dan Zhou

***Abstract*—Reconfiguration can increase the output power for a PV array under partial shadows. However, traditional reconfiguration methods consider the PV module as either totally shaded or totally unshaded, and module-based simulation is employed to evaluate the reconfiguration effect. Actually, there is an unneglectable error when treating a partially shaded PV module as totally shaded, through using a more accurate cell-based simulation. Based on the analysis of the determinant factors on MPPs' power of a PV array, a new reconfiguration method is proposed based on the exact partial shadow shape projected on the PV array. This method restructures the electrical connection among PV modules of a PV array according to the shaded cells' number (SCN) of every PV module. Extensive cell-based simulations are carried out on a PV array to verify the effectiveness of the proposed SCN-based reconfiguration method. Comprehensive comparisons among various reconfiguration methods and shadow distributions clearly show its suitability to different irregular shadows and its superiority in PV output power enhancement.**

***Index Terms*—Maximum power point (MPP), partial shadow, PV array, PV module, reconfiguration.**

I. Introduction

ACCORDING to the National Energy Administration, China's photovoltaic (PV) power generation capacity had reached 253 GW by the end of 2020, accounting for nearly 11.5% of the national total generation capacity. Limited by the installation area and panel cost of a PV array, improving the power generation efficiency of a PV system has become an important research field [1]–[4].

The structure of a PV array and the shape of a partial shadow are the two key factors affecting a PV system's output power. There are many interconnection schemes to form a PV array, such as Series-Parallel (SP), Total-Cross-Tied (TCT), Bridged-Link (BL), Honey-Comb (HC), Triple-Tied (TT), and various hybrid types evolving from them [5]. The TCT structure is a very popular scheme for output power enhancement under partial shading [6], [7]. In addition, the performance of a PV system depends largely on environmental conditions, such as clouds, buildings and other objects which will cast shadows on the PV arrays when the sun traverses the sky. This will result in irradiance loss across the PV surface and mismatch power loss among PV modules [8], [9]. The shadow shapes are usually irregular, and partially shaded PV modules are very common in PV arrays. In recent years, many reconfiguration techniques, including static and dynamic, have been proposed to mitigate the mismatch power loss in PV arrays [10]–[24].

For static reconfiguration, the power generation is increased by optimizing the physical locations or the electrical interconnections of PV modules before the PV system is put into operation. In [10], the PV modules in a TCT PV array are arranged by the SuDoKu puzzle pattern so as to distribute the shadow effect over the entire array. However, ineffective shade dispersion is experienced with the SuDoKu method [11]. Furthermore, in [12], an optimal SuDoKu reconfiguration method is proposed to reduce the wiring arrangement and increase the shading distribution over the array. In addition, the reconfiguration methods based on Futoshiki puzzle pattern [13], dominance square method [14] and LoShu technique [15] are put forward in succession to improve PV array power output. However, all of these above methods are only applicable to a square array. Furthermore, actual shadows change over time, and it is impossible for these static reconfiguration strategies to obtain the greatest power generation all the time.

Dynamic reconfiguration schemes can change the electrical connection of a PV array timely according to actual shadow conditions. In [16], the optimal reconfiguration of a PV array is formulated as a mixed integer quadratic programming problem, which is solved by the brand and bound algorithm. In [17], the grasshopper optimization algorithm is applied to the reconfiguration of a partially shaded PV array. In [18], the parallel computation is used in particle swarm optimization to achieve the best reconfiguration solution for a PV array. In [19], the "irradiance equalization" strategy is proposed to dynamically optimize the PV array's configuration. In [20], the series-voltage source is employed to make every PV branch operate on its own maximum power point (MPP). In [21], the two-step GA technique, based on a switching matrix, is proposed to overcome partial shading. In [22], a comparative study among all the published static and dynamic reconfiguration approaches and the challenges facing each approach are presented and discussed. To mitigate the high cost and complex wiring during dynamic reconfiguration, in [23], the electrical connections of a PV array is designed to interchange automatically between SP and TCT configurations under partial shading conditions; in [24] the optocoupler-based electronic circuit is designed for each PV module to avoid an

Manuscript received November 17, 2020; revised April 7, 2021, accepted July 24, 2021. Date of online publication May 6, 2022; date of current version March 6, 2023. This study was supported by the Key Research and Development Program of Zhejiang Province [grant number 2019C01149].

J. Qi (corresponding author, email: qijun@zjut.edu.cn), X. Huang, B. J. Ye and D. Zhou are with College of Information Engineering, Zhejiang University of Technology, Hangzhou 310014, China.

DOI: 10.17775/CSEEJPES.2020.06140

expensive sensing and complex switching network.

In all this research, the irregular partial shadow is simplified as a conjoining of the PV module's rectangular shape, which is at also commonly seen in other PV application fields at this time [25]. The difference between partially shaded and totally shaded on a PV module is ignored since it is difficult and incurs high-cost to obtain the exact shadow shape by conventional electrical sensors. Inspired by the successful image recognition of partial shadows on a PV array [26], the approximation error of irradiance equivalence for a partially shaded PV module is discussed in this paper. The dynamic reconfiguration strategy is redesigned according to the irregular shadow shape, which contains information about the shaded cells' number (SCN) of every PV module. Neither complex iteration computations, nor massive electrical sensors, are needed in this SCN-based method and it is applicable to PV arrays with different row and column sizes.

In our research, we focus on the reconfiguration algorithm, without considering reconfiguration costs on the switch matrix, wiring, etc. The remainder of this paper is organized as follows. Section II discusses the approximation error of conventional irradiance equivalence for partially shaded PV modules. The analysis of P-V peaks' number and the determinant factors on MPPs' output power are presented in Section III, followed by the new SCN-based reconfiguration method. Simulation results and discussions are provided in Section IV. Section V presents key conclusions.

II. Discussion of Partial Shadow Approximation Error

A. TCT PV Array Under Partial Shadow

Due to its low terminal voltage and output power, it is necessary to connect PV cells to form a PV module, and further connect PV modules together to form a PV array. As shown in Fig. 1, m-tier, n-column PV modules are connected as an $m \times n$ PV array of a TCT structure, and every PV module contains several PV cells in series inside. Each tier of the PV modules is connected with a bypass diode in parallel. The blocking diode is not considered here since maximum power point tracking (MPPT) in a properly reconfigured TCT PV array usually can avoid the reverse current. The PV module in tier x and column y is labeled as M_{xy}, where, $x = 1, 2, \cdots, m$, $y = 1, 2, \cdots, n$.

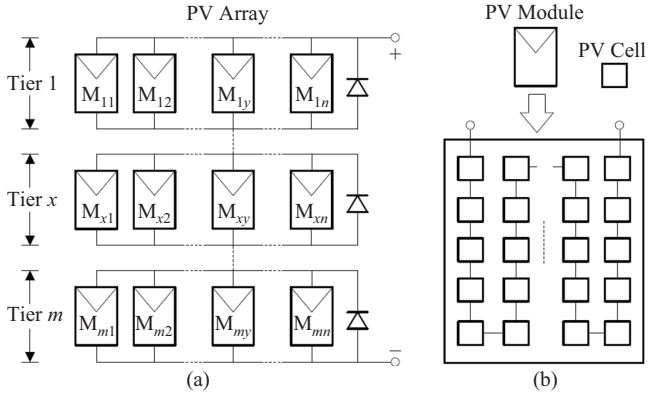

Fig. 1. Structure relationship between PV array, PV module and PV cell. (a) TCT structure of an $m \times n$ PV array; (b) series structure of a PV module.

When the PV array is suffering from irregular shadows, there are three possible PV module types: unshaded, totally shaded and partially shaded. In this paper, for simplicity, the irradiance within the shadow area is considered as uniform. Denote the irradiance in the unshaded area and shaded area as αW/m^2 and βW/m^2, respectively. Define the matrices $\boldsymbol{Q}$ and $\boldsymbol{P}$ as follows.

$$\boldsymbol{Q} = \begin{bmatrix} Q_{11} & \cdots & Q_{1n} \\ \vdots & \ddots & \vdots \\ Q_{m1} & \cdots & Q_{mn} \end{bmatrix} \tag{1}$$

$$\boldsymbol{P} = k \begin{bmatrix} 1 & \cdots & 1 \\ \vdots & \ddots & \vdots \\ 1 & \cdots & 1 \end{bmatrix} - \boldsymbol{Q} = \begin{bmatrix} P_{11} & \cdots & P_{1n} \\ \vdots & \ddots & \vdots \\ P_{m1} & \cdots & P_{mn} \end{bmatrix} \tag{2}$$

where the element Q_{xy} in the matrix $\boldsymbol{Q}$ is the shaded cells' number in the PV module M_{xy}, k is the total number of series PV cells in every PV module and the element P_{xy} in the matrix $\boldsymbol{P}$ is the unshaded cells' number.

Under the standard test condition (STC), the values of the short circuit current (I_{SC}) and the open circuit voltage (V_{OC}) have been tested and provided by the manufacturers. It should be noted that the irradiance and temperature will significantly affect the actual values of I_{SC} and V_{OC}. The temperature across a PV array surface is usually similar and thus is assumed to be uniform in this paper. The I_{SC} of a PV cell is proportional to the irradiance [27], therefore, when all the series PV cells in a PV module are connected with only one bypass diode outside, the I_{SC} of a partially shaded PV module is decided by the irradiance on its shaded cells. Meanwhile, the V_{OC} of a PV cell is in a logarithmic relationship with the irradiance [27], thus it will slightly decrease with the drop of irradiance. The V_{OC} of a PV module is the sum of the V_{OC} of all the PV cells in this module.

Denote the short circuit current as $I_{\mathrm{SC\_}\alpha}$ and $I_{\mathrm{SC\_}\beta}$, the open circuit voltage as $V_{\mathrm{OC\_}\alpha}$ and $V_{\mathrm{OC\_}\beta}$ for the PV cell under unshaded irradiance (i.e., αW/m^2) and shaded irradiance (i.e., βW/m^2), respectively. Based on the above analysis, the I_{SC}^{xy} and V_{OC}^{xy} of the PV module M_{xy} with Q_{xy} shaded cells and P_{xy} unshaded cells are given in (3).

$$\begin{cases} I_{\mathrm{SC}}^{xy} = \min(I_{\mathrm{SC\_}\alpha}, I_{\mathrm{SC\_}\beta}) = I_{\mathrm{SC\_}\beta} \\ V_{\mathrm{OC}}^{xy} = P_{xy} V_{\mathrm{OC\_}\alpha} + Q_{xy} V_{\mathrm{OC\_}\beta} \end{cases} \tag{3}$$

The PV modules of every tier in Fig. 1 are parallel-connected, the $I_{\mathrm{SC}x}$ and $V_{\mathrm{OC}x}$ of the Tier x can be calculated as in (4).

$$\begin{cases} I_{\mathrm{SC}x} = \sum_{y=1}^{n} I_{\mathrm{SC}}^{xy} \\ V_{\mathrm{OC}x} \approx \min\left(V_{\mathrm{OC}}^{x1}, V_{\mathrm{OC}}^{x2}, \cdots, V_{\mathrm{OC}}^{xn}\right) \end{cases} \tag{4}$$

B. Approximation Error in Partial Shadow Equivalence

Conventionally, a partially shaded PV module is often approximated as a totally shaded module for ease of simulation [28], [29]. In order to evaluate the shading degree or

shading strength of a PV module, the equivalent irradiance in (5) is introduced by references [9].

$$G_{xy} = \gamma \left[I_{xy} + I_0 \left(e^{V_{xy}/nV_T} - 1 \right) \right] \tag{5}$$

where G_{xy} is the equivalent irradiance of M_{xy}, I_{xy} and V_{xy} are the measured output current and voltage under present shadow conditions, respectively. γ, I_0 and nV_T can be evaluated from the PV module parameters under STC. The STC parameters of the PV modules in this section are presented in Appendix A.

Consider the 2×2 PV array in Fig. 2(a) where three PV modules are partially shaded with $\alpha = 1000$ W/m^2 and $\beta = 500$ W/m^2 in unshaded and shaded areas respectively. After irradiance equivalence, the partially shaded PV modules in Fig. 2(a) are now totally shaded in Fig. 2(b). The matrix $\boldsymbol{Q}$ of Array A & B are displayed in (6) and (7).

$$\boldsymbol{Q}_{\mathrm{A}} = \begin{bmatrix} 0 & 9 \\ 18 & 18 \end{bmatrix} \tag{6}$$

$$\boldsymbol{Q}_{\mathrm{B}} = \begin{bmatrix} 0 & 36 \\ 36 & 36 \end{bmatrix} \tag{7}$$

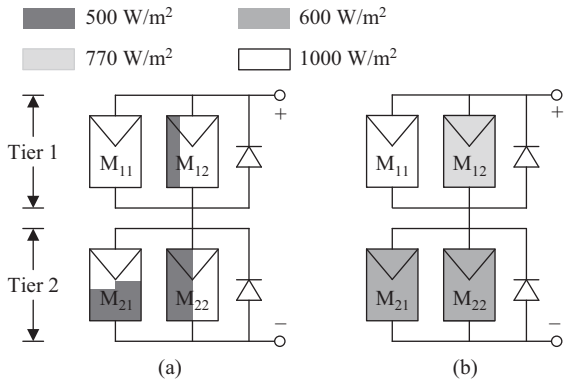

Fig. 2. Partially shaded PV array before and after irradiance equivalence: (a) Array A; (b) Array B.

By applying the MPP current and voltage of Array A to (5), the equivalent irradiance of M_{12} and M_{21}/M_{22} in Array B are 770 W/m^2 and 600 W/m^2, respectively. The characteristic curves of shaded modules before and after irradiance equivalence are plotted in Fig. 3 by cell-based simulation. Numerical results for comparison are listed in Table I. Since the shadow irradiance on M_{12} in Array A is lower than Array B, the I_{SC}^{12} in Array A is smaller than Array B according to (3), which is consistent with Fig. 3. The I_{SC}^{21} and I_{SC}^{22} are similar. In addition, there is an evident error in MPP power by treating a partially shaded module as totally shaded, especially for M_{12}.

It is worth noting that, in Array A, since the numbers of shaded cells in M_{21} and M_{22} are equal, the characteristic curves for them are identical, although the shadow shapes on them are different. Therefore, given the irradiance on a PV module, its output characteristic is determined by the number of shaded cells. It can be approximately considered that the number of shaded cells depends on the size of the shadow area. In the following discussions, for convenience, the irregular shadow shape on a PV module is uniformly represented as a rectangle area with the same size.

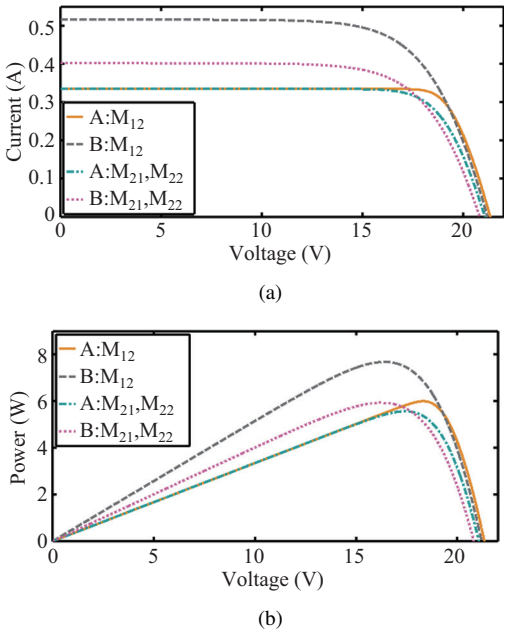

Fig. 3. Characteristic curves of shaded modules in Array A & B: (a) I-V curves; (b) P-V curves.

TABLE I
APPROXIMATION ERROR OF THE PARTIALLY SHADED PV MDOULES

Module	Array	I_{SC}^{xy} (A)	V_{OC}^{xy} (V)	P_{MPP}^{xy} [1] (W)	$\Delta P_{\mathrm{MPP}}^{xy}$ %[2]
M_{12}	A	0.335	21.33	6.00	–
	B	0.516	21.20	7.67	+27.83
M_{21}/M_{22}	A	0.335	21.06	5.56	–
	B	0.402	20.81	5.93	+6.65

[1] P_{MPP}^{xy} is the maximum power of the PV module M_{xy}.
[2] $\Delta P_{\mathrm{MPP}}^{xy}\% = (P_{\mathrm{MPP}}^{xy}|_{\mathrm{B}} - P_{\mathrm{MPP}}^{xy}|_{\mathrm{A}})/P_{\mathrm{MPP}}^{xy}|_{\mathrm{A}} \times 100$

To further illustrate the approximation error of irradiance equivalence on the whole PV array, the output characteristic curves of Array A & B are plotted in Fig. 4. It can be found that the MPP power of Array B is nearly 10% larger than Array A. This means that if we treat partially shaded modules as totally shaded, there is a considerable error in the MPP's power for the whole PV array. Therefore, it is reasonable and better to employ the cell-based simulation to obtain a more accurate result under irregular and partial shadows. Only in this way can we obtain more accurate and convincing results in comparing different reconfiguration methods.

III. SCN-BASED RECONFIGURATION PRINCIPLE

A. Analysis of P-V Peaks' Number

Due to the bypass diode, usually there are multiple peaks on the P-V curve of a partially shaded PV array before reconfiguration [30], [31]. The dynamic PV array (DPVA) is based on the TCT topology. For the DPVA shown in Fig. 5, the physical location of every PV module is fixed, while the electrical location of PV modules can be changed by the switching matrix similar to [32]. In Fig. 5, every PV module M_{xy} can be switched to connect with any electrical location by the switching matrix according to a reconfiguration strategy. It is worth noting that all the electrical locations

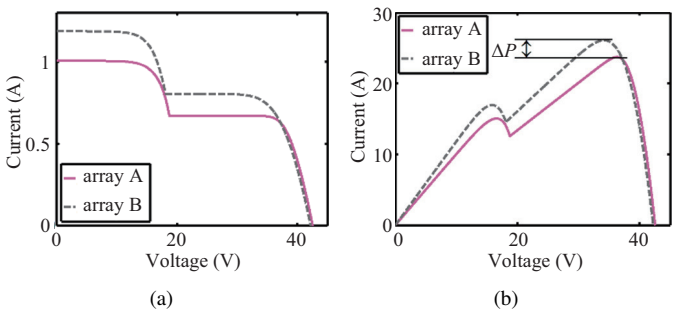

Fig. 4. Characteristic curves of Array A & B: (a) I-V curves; (b) P-V curves.

(e.g., $C_{i1}, C_{i2}, \cdots, C_{ij}, \cdots, C_{in}$ of the i_{th} tier $C_{i(1\sim n)}$) in any tier are electrically the same, and the sequence of tiers (e.g., $C_{1(1\sim n)}, \cdots, C_{i(1\sim n)}, \cdots, C_{m(1\sim n)}$) has no effect on the PV array's output.

In order to reduce the mismatch power loss, the irradiance differences between any two tiers of the TCT array should be minimized [16]. Under uniform shadow, it should distribute the shaded PV modules in each tier as evenly as possible. Suppose that there are $mc + d$ shaded modules in an $m \times n$ DPVA, where $c = 0, 1, 2, \cdots, n-1$ and $d = 0, 1, 2, \cdots, m$. There are two possible scenarios:

1) When $d = m$, there are $c+1$ shaded PV modules in each tier after reconfiguration. According to (3) and (4), the I_{SC} of each tier in the reconfigured PV array is equal. Therefore, there is only one step in the I-V curve and one peak in the P-V curve, for the reconfigured PV array.

2) When $d \neq m$, there are m-d tiers containing c shaded modules and d tiers containing $c + 1$ shaded modules after reconfiguration, which means that there are two different values for the tier's I_{SC}. Thus, for the reconfigured PV array, there are two steps in the I-V curve and two peaks in the P-V curve.

It can be concluded that no matter what the shadow shape is like, after distributing the shaded PV modules in each tier, as evenly as possible, there are at most two different levels of tier's I_{SC} in a PV array and thus at most two peaks in the P-V curve.

Mark the tiers with less shaded modules as "TWL, " and the tiers with more shaded modules as "TWM." Use Array A in Fig. 2(a) as an example. Obviously, Tier 1 in array A is TWL and Tier 2 is TWM. The I-V curves for Array A and its inner tiers are plotted in Fig. 6(a) by the cell-based simulation. The I-V curve of Array A has two steps, whose first step with lower voltage is determined by the TWL, while the second step with higher voltage is determined by the TWM. The P-V curve of Array A shown in Fig. 6(b) has two peaks, which from left to right are corresponding to the first and second step of Array A's I-V curve respectively. In other words, the left power peak is affected by the TWL and the right power peak is affected by the TWM.

B. Determinant Factors on MPPs' Power

Consider the 2×2 DPVA with irregular shadow distribution in Fig. 7(a), where M_{11} is totally shaded, M_{21} and M_{22} are partially shaded, and M_{12} is unshaded. The STC parameters of PV modules are listed in Appendix A. The matrix $\boldsymbol{Q}$ is shown in (8).

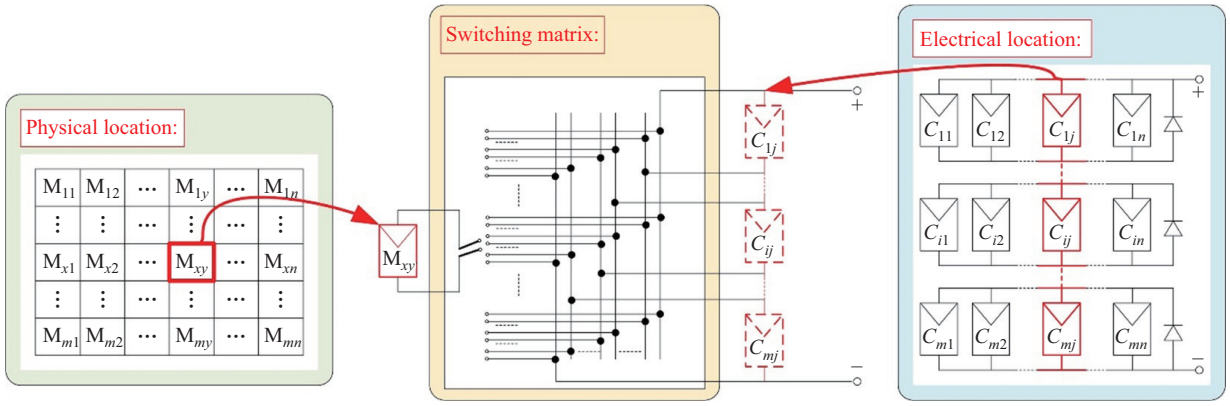

Fig. 5. Physical and electrical locations of PV modules in an $m \times n$ DPVA connected by a switching matrix.

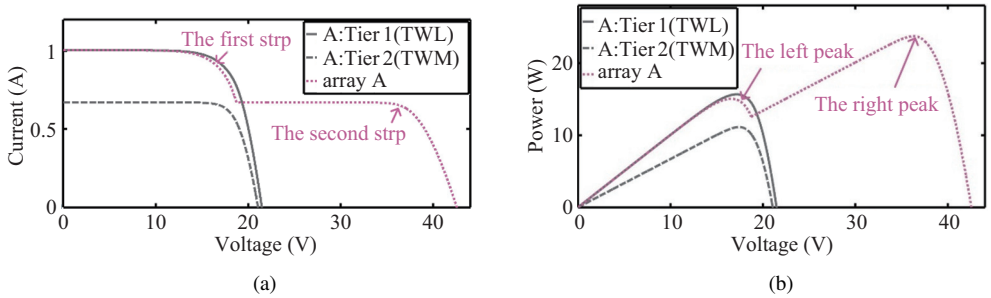

Fig. 6. Characteristic curves of Array A and its inner tiers: (a) I-V curves; (b) P-V curves.

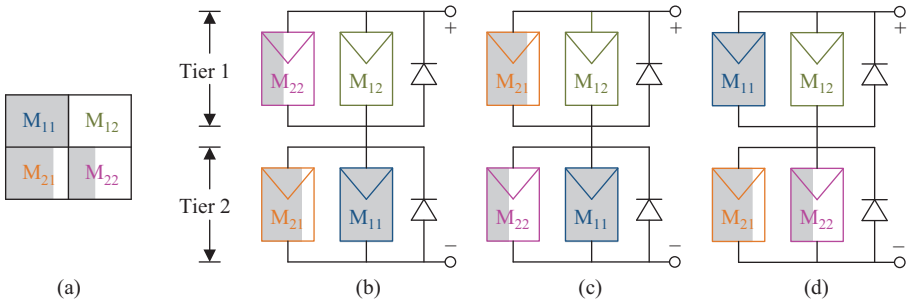

Fig. 7. The 2×2 DPVA with irregular shadow distribution and its possible electrical configurations: (a) Irregular shadow distribution; (b) EC1; (c) EC2; (d) EC3.

$$\boldsymbol{Q} = \begin{bmatrix} Q_{11} & Q_{12} \\ Q_{21} & Q_{22} \end{bmatrix} = \begin{bmatrix} 36 & 0 \\ 27 & 15 \end{bmatrix} \tag{8}$$

It is well-known that whether there is an up and down exchange between tiers or a left and right exchange in every tier, it will not change the electrical characteristics of the TCT PV array. Therefore, the PV array shown in Fig. 7(a) can be reconfigured to three different electrical configurations, which are shown in Fig. 7(b)–(d), marked as EC_1, EC_2 and EC_3 respectively. In a conventional reconfiguration, these three electrical configurations are considered the same.

From Fig. 7(b)–(d), it can be seen that Tier 2 contains one more shaded module than Tier 1. Therefore, Tier 1 is taken as *TWL* and Tier 2 as *TWM*. The differences among EC_1, EC_2 and EC_3 are the electrical location of partially shaded PV modules: M_{11}, M_{21} and M_{22}. Denote $Q_x(\mathrm{EC}_w)$ as the total number of shaded cells of Tier x in EC_w, where $w = 1$, 2, 3. Based on (8), we have:

$$\text{Tier 1}(\textit{TWL}) Q_1(\mathrm{EC}_3) > Q_1(\mathrm{EC}_2) > Q_1(\mathrm{EC}_1) \tag{9}$$

$$\text{Tier 2}(\textit{TWM}) Q_2(\mathrm{EC}_1) > Q_2(\mathrm{EC}_2) > Q_2(\mathrm{EC}_3) \tag{10}$$

According to (3), the I_{SC} and V_{OC} of these PV modules fulfill the following relationships:

$$\begin{cases} I_{\mathrm{SC}}^{12} > I_{\mathrm{SC}}^{11} = I_{\mathrm{SC}}^{21} = I_{\mathrm{SC}}^{22} \\ V_{\mathrm{OC}}^{12} > V_{\mathrm{OC}}^{22} > V_{\mathrm{OC}}^{21} > V_{\mathrm{OC}}^{11} \end{cases} \tag{11}$$

According to (4), the short circuit current $I_{\mathrm{SC}x}(EC_w)$ and the open circuit voltage $V_{\mathrm{OC}x}(\mathrm{EC}_w)$ of Tier x in EC_w further fulfill the following relationships:

$$\text{Tier 1 } (\textit{TWL}) \begin{cases} I_{\mathrm{SC1}}(\mathrm{EC}_1) = I_{\mathrm{SC1}}(\mathrm{EC}_2) = I_{\mathrm{SC1}}(\mathrm{EC}_3) \\ V_{\mathrm{OC1}}(\mathrm{EC}_1) > V_{\mathrm{OC1}}(\mathrm{EC}_2) > V_{\mathrm{OC1}}(\mathrm{EC}_3) \end{cases} \tag{12}$$

$$\text{Tier 2 } (\textit{TWM}) \begin{cases} I_{\mathrm{SC2}}(\mathrm{EC}_1) = I_{\mathrm{SC2}}(\mathrm{EC}_2) = I_{\mathrm{SC2}}(\mathrm{EC}_3) \\ V_{\mathrm{OC2}}(\mathrm{EC}_3) > V_{\mathrm{OC2}}(\mathrm{EC}_2) = V_{\mathrm{OC2}}(\mathrm{EC}_1) \end{cases} \tag{13}$$

Consider the above conclusions that the left peak of the P-V curve is primarily affected by *TWL*, whereas the right peak is primarily affected by *TWM*. $P_{\mathrm{MPP\_L}}(\mathrm{EC}_w)$ and $P_{\mathrm{MPP\_R}}(\mathrm{EC}_w)$ denote the power value of the left and right peak in EC_w respectively. Combining (9) and (12), for the *TWL* case, the number of shaded cells in EC_1 is the least among all the three electrical configurations, so that EC_1 has the largest left peak's power value. Combining (10) and (13), for the *TWM* case, the number of shaded cells in EC_3 is the least, so that the right peak's power value of EC_3 is the largest. Then, we have:

$$P_{\mathrm{MPP\_L}}(\mathrm{EC}_1) > P_{\mathrm{MPP\_L}}(\mathrm{EC}_2) > P_{\mathrm{MPP\_L}}(\mathrm{EC}_3) \tag{14}$$

$$P_{\mathrm{MPP\_R}}(\mathrm{EC}_3) > P_{\mathrm{MPP\_R}}(\mathrm{EC}_2) \approx P_{\mathrm{MPP\_R}}(\mathrm{EC}_1) \tag{15}$$

To check the validity of the above analysis, cell-based simulations are performed and compared for EC_1, EC_2 and EC_3. Set $\alpha = 1000$ W/m^2 and $\beta = 200$ W/m^2, respectively. The P-V curves of EC_1, EC_2 and EC_3 are plotted in Fig. 8. Part of the results are shown in Table II. It can be seen that EC_1 has the highest left peak whereas EC_3 has the highest right peak, which coincide with the analysis results above. Thus, we have these conclusions:

1) The less shaded cells in *TWL*, the higher the left peak on the P-V curve.
2) The less shaded cells in *TWM*, the higher the right peak on the P-V curve.

TABLE II
COMPARISON OF MPPS' POWER FOR EC_1, EC_2 AND EC_3

Electrical Configuration	$P_{\mathrm{MPP\_L}}$ (W)	$P_{\mathrm{MPP\_R}}$ (W)	P_{MPP} (W)	P_{MPP} change w.r.t. EC_3 (%)
EC_1	11.70	8.97	11.70	+4.09
EC_2	11.50	8.99	11.50	+2.31
EC_3	11.24	9.32	11.24	–

There is up to a 4% power increase from EC3 to EC1. Taken these differences among partially shaded PV modules into consideration, the conventional reconfiguration methods can be further improved. With the help of shadow image recognition techniques, it is possible to figure out the shaded cells' number in every PV module. Thus, it is easy to carry out the new SCN-based reconfiguration method as illustrated in the next section.

C. SCN-Based Reconfiguration Flowchart

From Section III-A and III-B, we can summarize that:

1) There are at most two peaks on the P-V curve after distributing shaded modules (including totally or partially shaded) in each tier as evenly as possible;
2) Less shaded cells in the *TWL*/*TWM* leads to a higher left/right power peak on the P-V curve.

In order to obtain a higher global MPP for the DPVA, the relatively less shaded PV modules should be placed in TWL or

TWM as much as possible. By comparing the two schemes, the one with a larger global MPP is the final choice. The flowchart of the SCN-based reconfiguration method is shown in Fig. 9, including the following 8 steps:

Step 1: Set initial condition

Start from sunrise time, define a DPVA formed by $m \times n$PV modules, and record the current electrical configuration as EC_0.

Step 2: Determine the matrix $\boldsymbol{Q}$

By shadow shape recognition, recognize the shaded PV modules and compute the number of shaded cells of every PV module. If all the elements Q_{xy} $(x = 1, 2, \cdots, m;$ $y = 1, 2, \cdots, n)$ in matrix $\boldsymbol{Q}$ are 0, which means that the PV array is not shaded, then go to Step 7, otherwise go to Step 3.

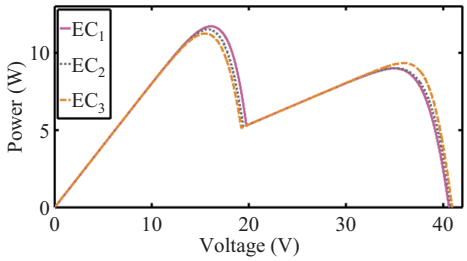

Fig. 8. P-V curves for EC_1, EC_2 and EC_3 in Fig. 7(b)–(d).

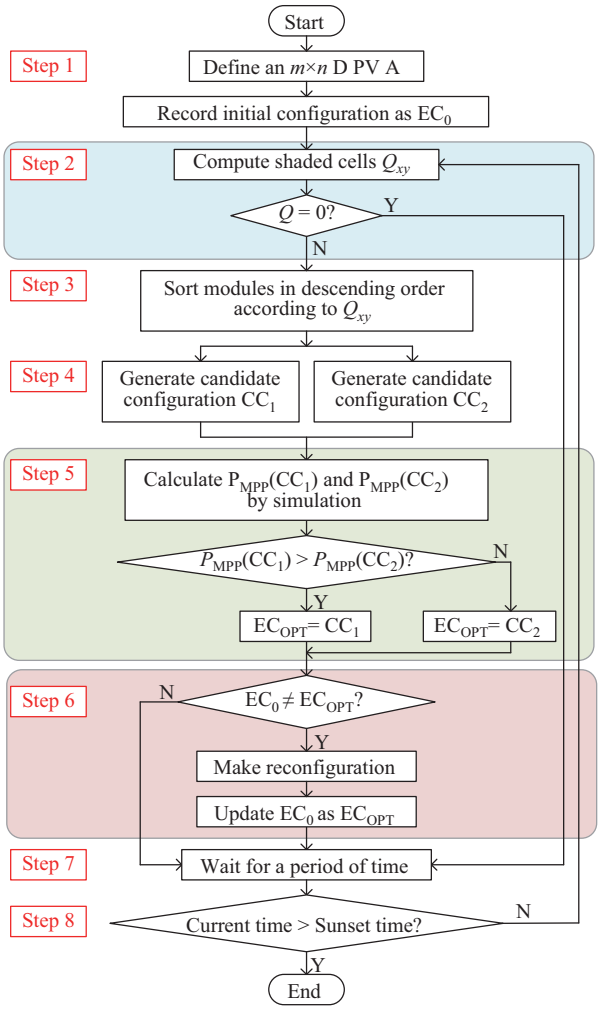

Fig. 9. Flowchart of the SCN-based reconfiguration method.

Step 3: Sort shaded modules by Q_{xy}

Assume that the total number of shaded modules is $mc+d$, where $c = 0, 1, 2, \cdots, n-1$ and $d = 0, 1, 2, \cdots, m$. Sort the shaded modules in descending order according to the value of Q_{xy}. The sequence obtained is denoted as l in (16).

$$l = \{S_1, S_2, S_3, \cdots, S_{mc+d}\} \tag{16}$$

where S_1 is the module with maximum value of Q_{xy}, S_{mc+d} is with minimum value of Q_{xy}. After distributing these shaded modules in each tier as evenly as possible, there will be m-d tiers in TWL and d tiers in TWM.

Step 4: Generate candidate electrical configurations

Candidate configuration 1 (CC_1) shown in Fig. 10(a): Put the less shaded modules from $S_{d(c+1)+1}$ to S_{mc+d} in TWL, and put the more shaded modules left in TWM.

Candidate configuration 2 (CC_2) shown in Fig. 10(b): Put the less shaded modules from $S_{(m-d)c+1}$ to S_{mc+d} in TWM, and put the more shaded modules left in TWL.

The distribution of non-shaded modules in CC_1 or CC_2 will not affect the DPVA's electrical output, so it is simplified in this research.

Step 5: Compute and compare GMPPs

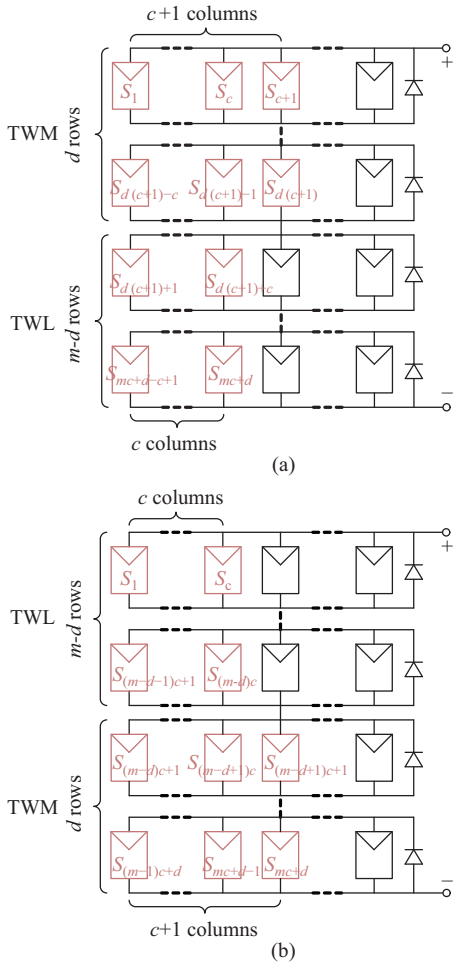

Fig. 10. Two candidate configurations for the DPVA under the same shadow: (a) CC1; (b) CC2.

Calculate the exact GMPP's power $P_{\mathrm{MPP}}(\mathrm{CC}_1)$ and $P_{\mathrm{MPP}}(\mathrm{CC}_2)$ for CC_1 and CC_2 by the cell-based simulation respectively. The configuration with larger GMPP's power is chosen as the optimal one, and defined as $\mathrm{EC}_{\mathrm{OPT}}$.

Step 6: Perform the reconfiguration

If $\mathrm{EC}_{\mathrm{OPT}}$ is different from EC_0, the DPVA is reconfigured in terms of $\mathrm{EC}_{\mathrm{OPT}}$ and EC_0 is updated as $\mathrm{EC}_{\mathrm{OPT}}$, otherwise enters Step 7 directly.

Step 7: Wait for a period of time

After one round of reconfiguration, it takes a period of time to wait for the change of shadow.

Step 8: Judge the end of reconfiguration

If the current time is later than the sunset time, the reconfiguration algorithm will be ended for one day, otherwise go to Step 2 for the next round of reconfiguration.

IV. Simulation and Discussion

A. Validation of the SCN-based Reconfiguration

To check the validity of the proposed SCN-based reconfiguration method, a 5×5 DPVA is constructed by adopting the PV module TSM-195DC01 A made by TrinaSolar. The modules' STC parameters are presented in Appendix B. Fig. 11(a) is the irregular shadow distribution on this DPVA's physical location, and the initial electrical configuration (EC_0) is shown in Fig. 11(b). The number of shaded cells on every PV module is given by matrix $\boldsymbol{Q}$:

$$\boldsymbol{Q}=\begin{bmatrix}0&1&0&0&0\\17&55&41&33&3\\37&72&72&72&33\\24&72&56&60&52\\4&21&5&7&15\end{bmatrix} \tag{17}$$

The sequence l in (16) after sorting is as follows:

$$\begin{aligned}l=\{&\mathrm{M}_{42},\mathrm{M}_{34},\mathrm{M}_{33},\mathrm{M}_{32},\mathrm{M}_{44},\mathrm{M}_{43},\mathrm{M}_{22},\\&\mathrm{M}_{45},\mathrm{M}_{23},\mathrm{M}_{31},\mathrm{M}_{35},\mathrm{M}_{24},\mathrm{M}_{41},\mathrm{M}_{52},\\&\mathrm{M}_{21},\mathrm{M}_{55},\mathrm{M}_{54},\mathrm{M}_{53},\mathrm{M}_{51},\mathrm{M}_{25},\mathrm{M}_{12}\}\end{aligned} \tag{18}$$

By putting the less shaded modules in TWL or TWM, two candidate electrical configurations CC_1 and CC_2 are shown in Fig. 11(c) and Fig. 11(d) respectively. When $\alpha=1000$ W/m^2 and $\beta=200$ W/m^2, through cell-based simulation, the P-V curves of EC_0, CC_1 and CC_2 are presented in Fig. 12. Part of the simulation results are provided in Table III. It can be seen that CC_2 generates more MPP power than CC_1. So record CC_2 as $\mathrm{EC}_{\mathrm{OPT}}$, and reconfigure EC_0 in terms of $\mathrm{EC}_{\mathrm{OPT}}$. By reconfiguration, the MPP power is increased by 33.52% compared with EC_0. In addition, there is about 2% increase from CC_1 to CC_2, which are considered as the same in conventional reconfigurations.

TABLE III
Power Change of CC_1, CC_2 with Respect to EC_0

Electrical Configuration	P_{MPP} (W)	Power change w.r.t. EC_0 (%)
EC_0	1070.6	–
CC_1	1408.2	+31.53
CC_2	1429.5	+33.52

B. Comparison of Reconfiguration Methods

To further evaluate the SCN-based method, another two reconfiguration methods are employed for comparison. One is the Dominance Square (DS) method in [14] and the other is the Optimized Irradiance Equalization (OIE) method in [19]. The DS method follows the dominant square puzzle pattern for number placement in a square matrix. The OIE method adopts an iterative and hierarchical sorting algorithm to establish a near optimum configuration. Just like other conventional reconfiguration techniques, none of them distinguishes between partially shaded and totally shaded PV modules. By changing the irradiance values of α and β respectively, two groups of cell-based simulations are carried out, and the power increase effect of SCN, OIE and DS are compared in Fig. 13.

Case 1: Take $\alpha=1000$ W/m^2, the value of β varies from 200 W/m^2 to 600 W/m^2.

Case 2: Take $\beta=200$ W/m^2, the value of α varies from 400 W/m^2 to 800 W/m^2.

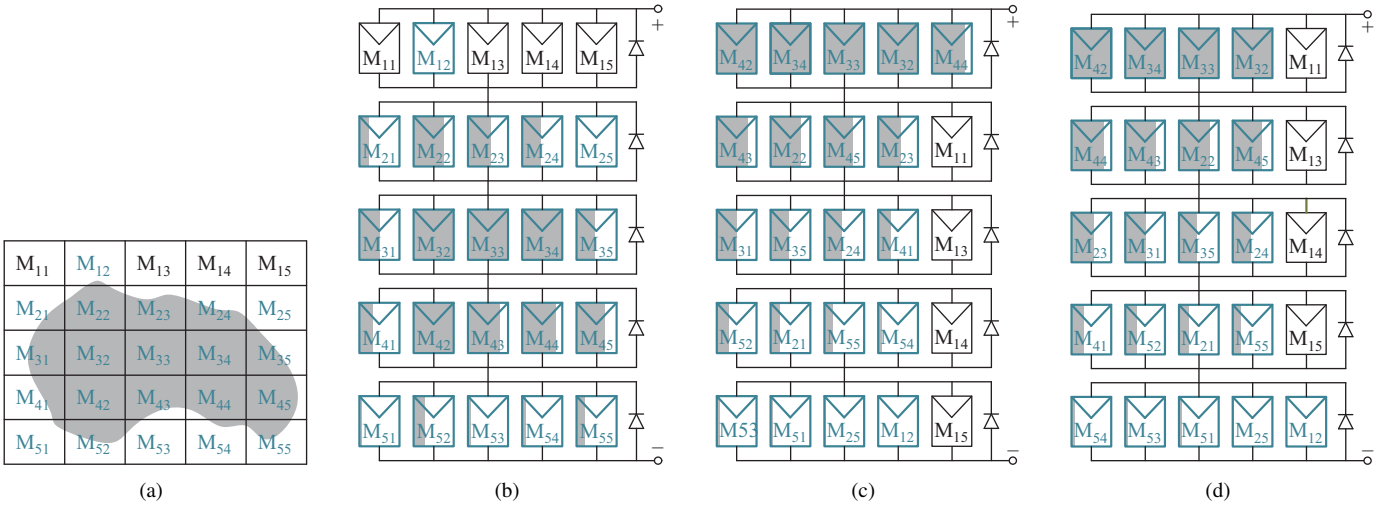

Fig. 11. Shadow distributions on DPVA and its different electrical configurations. (a) Irregular shadow distribution on the 5×5 DPVA's physical location; (b) initial electrical configuration (EC_0); (c) candidate configuration 1 (CC_1); (d) candidate configuration 2 (CC_2).

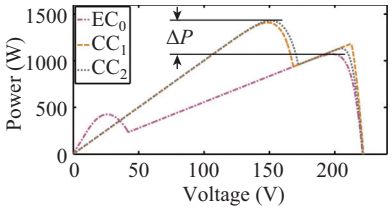

Fig. 12. P-V curves of different electrical configurations.

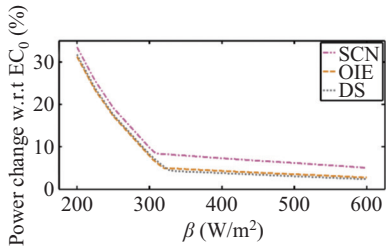

(a)

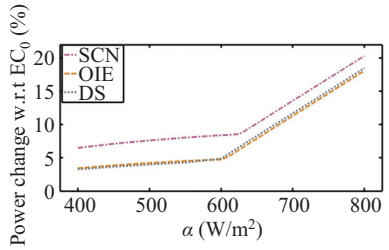

(b)

Fig. 13. Comparison of power increases by adopting different reconfiguration methods for (a) Case 1; (b) Case 2.

From Fig. 13(a), it can be found that for Case 1 with $\alpha = 1000$ W/m^2 fixed, when $\beta > 300$ W/m^2, the power rise by adopting SCN method is about two times larger than that by the OIE and DS methods. When $\beta < 300$ W/m^2, although all the three methods provide satisfactory power enhancement, the SCN method performs best. From Fig. 13(b), for Case 2 with $\beta = 200$ W/m^2 fixed, when $\alpha < 600$ W/m^2, SCN method provides more than 6.5% power enhancement which is two times larger than that of the OIE and DS methods. When $\alpha > 600$ W/m^2, although all the three methods can greatly increase the output power, the improvement by the OIE method or DS method are obviously smaller than the SCN method. The above analysis indicates that the proposed SCN reconfiguration is superior in raising the output power of the PV array under irregular shadow.

In addition, it is worth noting that the DS method is only applicable to a square array. In the OIE method, a lot of sensors are needed to measure the voltage and the current of each module, and iterations are needed in the reconfiguration process. In addition, the OIE method requires the row number of the PV array to be a power of two. In contrast, for the proposed SCN method, there is no iteration for every reconfiguration round and it is applicable to the arbitrary size of the PV array. Therefore, the SCN method is easier to implement and more adaptable than the OIE method.

C. Test under Different Shadow Distributions

Three different patterns of shadow distributions are shown in Fig. 14 to simulate partial shadows caused by mountains, buildings and trees around the PV array or bird droppings, surface dirt and clouds above the PV array. They are the Short-Wide (SW) shadow, Long-Narrow (LN) shadow and Discontinuous (DIS) shadow, respectively. The total number of shaded cells in these shadow distributions is set as equal. Similar to the two case settings in Section 4.2, simulations are carried out by varying irradiance values of α and β, respectively. The results are presented in Fig. 15.

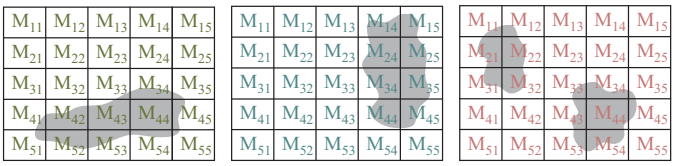

(a) (b) (c)

Fig. 14. Shading patterns: (a) Short-Wide (SW) shadow; (b) Long-Narrow (LN) shadow; (c) Discontinuous (DIS) shadow.

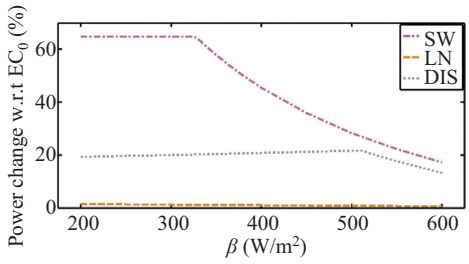

(a)

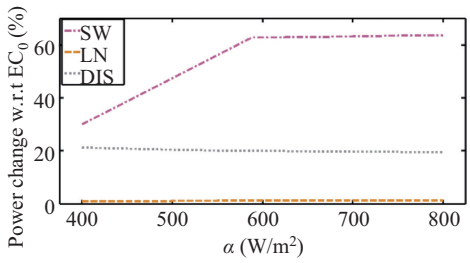

(b)

Fig. 15. Comparison of power increase under different shading patterns for (a) Case 1; (b) Case 2.

For the PV array under the SW shadow, the SCN method provides the best output power enhancement. From Fig. 15(a), when $\beta < 350$ W/m^2, the power is increased by more than 60%. When $\beta > 350$ W/m^2, as β rises, the power enhancement decreases. From Fig. 15(b), when $\alpha > 600$ W/m^2, the power is increased by more than 60%. When $\alpha < 600$ W/m^2, as α drops, the power enhancement decreases. The reason for the apparent power rise is that the mismatch power under the SW shadow is relatively the largest. After reconfiguration, the impact of the mismatch can be greatly reduced. For the PV array under the DIS shadow, the power can be improved by about 20%. For the PV array under the LN shadow, the power improvement is negligible as the mismatch power loss of the

PV array under the LN shadow is the smallest. In other words, the current configuration is close to the optimum one.

V. Conclusion

By adopting the cell-based simulation, the approximation error caused by the conventional module-based simulation after irradiance equivalence is exposed and compared. After the detailed analysis of the P-V curve features under partial shadow, a SCN-based reconfiguration method is designed to optimize the electrical connections among PV modules. Rather than requiring complex iterative algorithms, this reconfiguration method only requires a simple SCN sort process which is welcome in engineering applications. The cell-based simulations carried out under different partial shadows reveals a large amount of output power increase after the PV array reconfiguration. By comparing the ability of power enhancement under different shadow distributions, this SCN-based method is shown to be obviously superior against the conventional methods.

However, there are a lot of switches and wires needed by the DPVA to implement reconfiguration, and it is still a long way until large-scale commercial applications for PV array reconfiguration technology are feasible. How to simplify the DPVA wiring structure and cut down the number of switches, and meanwhile maintain the power enhancement ability under complex shadow types, is still a huge obstacle to be overcome in the future.

Appendix A

PV Module (GHM10W) Data under STC

Number of series cells = 36
Nominal DC power = 10 W
Voltage at nominal power = 17.6 V
Current at nominal power = 0.57 A
Open circuit voltage = 21.6 V
Short circuit current = 0.67 A

Appendix B

PV Module (TSM-195DC01A) Data under STC

Number of series cells = 72
Nominal DC power = 195 W
Voltage at nominal power = 37.1 V
Current at nominal power = 5.25 A
Open circuit voltage = 45.6 V
Short circuit current = 5.56 A

References

[1] D. Q. Zhou, Z. T. Chong, and Q. W. Wang, "What is the future policy for photovoltaic power applications in China? Lessons from the past. *Resources Policy*, vol. 65, pp. 101575, Mar. 2020.

[2] D. T. Thayalan, H. S. Lee, and J. H. Park, "Low-cost high-efficiency discrete current sensing method using bypass switch for PV systems," *IEEE Transactions on Instrumentation and Measurement*, vol. 63, no. 4, pp. 769–780, Apr. 2014.

[3] J. Qi, Y. B. Zhang, and Y. Chen, "Modeling and maximum power point tracking (MPPT) method for PV array under partial shade conditions," *Renewable Energy*, vol. 66, pp. 337–345, Jun. 2014.

[4] A. A. Elserougi, M. S. Diab, A. M. Massoud, A. S. Abdel-Khalik, and S. Ahmed, "A switched PV approach for extracted maximum power enhancement of PV arrays during partial shading," *IEEE Transactions on Sustainable Energy*, vol. 6, no. 3, pp. 767–772, Jul. 2015.

[5] P. K. Bonthagorla and S. Mikkili, "Performance investigation of hybrid and conventional PV array configurations for grid-connected/standalone PV systems," *CSEE Journal of Power and Energy Systems*, vol. 8, no. 3, pp. 682–695, May 2022, doi: 10.17775/CSEEJPES.2020.02510.

[6] O. Bingöl and B. Özkaya, "Analysis and comparison of different PV array configurations under partial shading conditions," *Solar Energy*, vol. 160, pp. 336–343, Jan. 2018.

[7] L. F. L. Villa, D. Picault, B. Raison, S. Bacha, and A. Labonne, "Maximizing the power output of partially shaded photovoltaic plants through optimization of the interconnections among its modules," *IEEE Journal of Photovoltaics*, vol. 2, no. 2, pp. 154–163, Apr. 2012.

[8] G. Petrone, G. Spagnuolo, R. Teodorescu, M. Veerachary, and M. Vitelli, "Reliability issues in photovoltaic power processing systems," *IEEE Transactions on Industrial Electronics*, vol. 55, no. 7, pp. 2569–2580, Jul. 2008.

[9] J. Storey, P. R. Wilson, and D. Bagnall, "The optimized-string dynamic photovoltaic array," *IEEE Transactions on Power Electronics*, vol. 29, no. 4, pp. 1768–1776, Apr. 2014.

[10] B. I. Rani, G. S. Ilango, and C. Nagamani, "Enhanced power generation from PV array under partial shading conditions by shade dispersion using Su Do Ku configuration," *IEEE Transactions on Sustainable Energy*, vol. 4, no. 3, pp. 594–601, Jul. 2013.

[11] S. R. Potnuru, D. Pattabiraman, S. I. Ganesan, and N. Chilakapati, "Positioning of PV panels for reduction in line losses and mismatch losses in PV array," *Renewable Energy*, vol. 78, pp. 264–275, Jun. 2015.

[12] S. G. Krishna and T. Moger, "Optimal SuDoKu reconfiguration technique for Total-Cross-Tied PV array to increase power output under non-uniform irradiance," *IEEE Transactions on Energy Conversion*, vol. 34, no. 4, pp. 1973–1984, Dec. 2019.

[13] H. S. Sahu, S. K. Nayak, and S. Mishra, "Maximizing the power generation of a partially shaded PV array," *IEEE Journal of Emerging and Selected Topics in Power Electronics*, vol. 4, no. 2, pp. 626–637, Jun. 2016.

[14] B. Dhanalakshmi and N. Rajasekar, Dominance square based array reconfiguration scheme for power loss reduction in solar Photovoltaic (PV) systems," *Energy Conversion and Management*, vol. 156, pp. 84–102, Jan. 2018.

[15] R. Venkateswari and N. Rajasekar, "Power enhancement of PV system via physical array reconfiguration based Lo Shu technique," *Energy Conversion and Management*, vol. 215, pp. 112885, Jul. 2020.

[16] M. Z. S. El-Dein, M. Kazerani, and M. M. A. Salama, "Optimal photovoltaic array reconfiguration to reduce partial shading losses," *IEEE Transactions on Sustainable Energy*, vol. 4, no. 1, pp. 145–153, Jan. 2013.

[17] A. Fathy, "Recent meta-heuristic grasshopper optimization algorithm for optimal reconfiguration of partially shaded PV array," *Solar Energy*, vol. 171, pp. 638–651, Sep. 2018.

[18] T. S. Babu, J. P. Ram, T. Dragičević, M. Miyatake, F. Blaabjerg, and N. Rajasekar, "Particle swarm optimization based solar PV array reconfiguration of the maximum power extraction under partial shading conditions," *IEEE Transactions on Sustainable Energy*, vol. 9, no. 1, pp. 74–85, Jan. 2018.

[19] J. P. Storey, P. R. Wilson, and D. Bagnall, "Improved optimization strategy for irradiance equalization in dynamic photovoltaic arrays," *IEEE Transactions on Power Electronics*, vol. 28, no. 6, pp. 2946–2956, Jun. 2013.

[20] W. J. Zhu and F. Rong, "Structural design of photovoltaic arrays based on series-voltage source under partial shading," *Proceedings of the CSEE*, vol. 33, pp. 96–103, Dec. 2013.

[21] A. M. Ajmal, V. K. Ramachandaramurthy, A. Naderipour, and J. B. Ekanayake, "Comparative analysis of two-step GA-based PV array reconfiguration technique and other reconfiguration techniques," *Energy Conversion and Management*, vol. 230, pp. 113806, Feb. 2021.

[22] A. M. Ajmal, T. S. Babu, V. K. Ramachandaramurthy, D. Yousri, and J. B. Ekanayake, "Static and dynamic reconfiguration approaches for mitigation of partial shading influence in photovoltaic arrays," *Sustainable Energy Technologies and Assessments*, vol. 40, pp. 100738, Aug. 2020.

[23] R. Pachauri, R. Singh, A. Gehlot, R. Samakaria, and S. Choudhury, "Experimental analysis to extract maximum power from PV array reconfiguration under partial shading conditions," *Engineering Science and Technology, an International Journal*, vol. 22, no. 1, pp. 109–130, Feb. 2019.

[24] A. F. Murtaza, H. A. Sher, K. Al-Haddad, and F. Spertino, "Module level electronic circuit based PV array for identification and reconfiguration of bypass modules," *IEEE Transactions on Energy Conversion*, vol. 36, no. 1, pp. 380–389, Mar. 2021.
[25] M. V. Rocha, L. P. Sampaio, and S. A. O. da Silva, "Comparative analysis of MPPT algorithms based on Bat algorithm for PV systems under partial shading condition," *Sustainable Energy Technologies and Assessments*, vol. 40, pp. 100761, Aug. 2020.
[26] B. J. Ye, J. Qi, Y. C. Li, L. Y. Xie, and F. Yang, "Research on PV array output characteristics based on shadow image recognition," in *Proceedings of 2017 IEEE Conference on Energy Internet and Energy System Integration*, Beijing, China, 2017, pp. 1–6.
[27] D. S. Feng, J. L. Song, H. Zhao, S. Lin, and H. B. Zhao, "*Theory and Application of Solar Power Generation*. Beijing: Posts & Telecom Press, 2007, pp. 44–48.
[28] P. Kuhn, M. Wirtz, S. Wilbert, J. L. Bosch, G. Wang, L. Ramirez, D. Heinemann, and R. Pitz-Paal, "Field validation and benchmarking of a cloud shadow speed sensor," *Solar Energy*, vol. 173, pp. 229–245, Oct. 2018.
[29] S. Mohammadnejad, A. Khalafi, and S. M. Ahmadi, "Mathematical analysis of total-cross-tied photovoltaic array under partial shading condition and its comparison with other configurations," *Solar Energy*, vol. 133, pp. 501–511, Aug. 2016.
[30] H. Y. Zheng, S. H. Li, R. Challoo, and J. Proano, "Shading and bypass diode impacts to energy extraction of PV arrays under different converter configurations," *Renewable Energy*, vol. 68, pp. 58–66, Aug. 2014.
[31] S. Sajadian and R. Ahmadi, "Distributed maximum power point tracking using model predictive control for photovoltaic energy harvesting architectures based on cascaded power optimizers," *IEEE Journal of Photovoltaics*, vol. 7, no. 3, pp. 849–857, May 2017.
[32] B. K. Karmakar and G. Karmakar, "A current supported PV array reconfiguration technique to mitigate partial shading," *IEEE Transactions on Sustainable Energy*, vol. 2, no. 2, pp. 1449–1460, Apr. 2021.

Jun Qi received her B.S. and Ph.D. degrees from Zhejiang University, Hangzhou, China, in 2004 and 2009, respectively. Now she is an associate professor in Zhejiang University of Technology, Hangzhou, China. Her research interests include renewable energy generation, power system analysis and control.

Xun Huang received the B.S. degree from Zhejiang University of Technology, Hangzhou, China, in 2020. He is currently pursuing his M.S. degree at Zhejiang University of Technology, Hangzhou, China. His research interests include new energy generation technology and PV power prediction.

Beijia Ye received her M.S. degree from Zhejiang University of Technology, Hangzhou, China, in 2019. Her research interests include smart grid and PV power generation.

Dan Zhou received his B.S. and Ph.D. degrees from Zhejiang University, Hangzhou, China, in 2006 and 2011, respectively. From 2011 to 2016, he was a Senior Engineer, a Project Manager, and the Director with State Grid Zhejiang Electric Power Co., Ltd. Electric Power Research Institute, Hangzhou, China. From 2016, He is with the Department of Electrical Engineering, Zhejiang University of Technology, Hangzhou, China. His current research interests include distributed generation and power system, especially planning of microgrids, optimization methods, and demand response.